Exact thermoelastic analysis of a thick cylindrical functionally graded material shell under unsteady heating using first order shear deformation theory

Vaziri, SA, Ghannad, M and Beg, OA

http://dx.doi.org/10.1002/htj.21455

HEAT TRANSFER-ASIAN RESEARCH

Accepted March 11th 2019

Online ISSN:1523-1496; Publisher – Wiley.

EXACT THERMOELASTIC ANALYSIS OF A THICK CYLINDRICAL FGM SHELL UNDER UNSTEADY HEATING USING FIRST ORDER SHEAR DEFORMATION THEORY

***Seyyed Amirreza Vaziri[1], Mehdi Ghannad[2] and O. Anwar Bég[3]**

1- Ph. D. Student, Faculty of Mechanical Engineering, Shahrood University of Technology, Shahrood, Iran.
2- Associate Professor, Faculty of Mechanical Engineering, Shahrood University of Technology, Shahrood, Iran
3- Multi-Physical Engineering Sciences, Mechanical and Aeronautical Engineering, University of Salford, Manchester, M54WT, UK.

****Corresponding Author-Email: Vaziri92amirreza@gmail.com***

P.O.B. 3619995161, Shahrood, Iran.

ABSTRACT

In this article, a new analytical formulation is presented for axisymmetric thick-walled FGM cylinder with power-law variation in mechanical and thermal properties under transient heating using first order shear deformation theory. Equilibrium equations are derived by virtual work principles and energy method. The unsteady heat conduction equation is solved using the method of separation of variables, generalized Bessel functions and an Eigen-function method. Validation of the analytical solutions is conducted with a finite element method (FEM). The effects of time on stress and displacement distribution are studied in detail. The numerical values used in this study are selected based on earlier studies. The influence of effect of transient heat transfer on heterogeneous thick-walled cylinder elasticity is clearly demonstrated. In particular the significant influence of time and heterogenous constant on radial displacement, hoop stress and temperature distributions is computed. The study is relevant to rocket chamber thermo-mechanics, propulsion duct thermophysical design, industrial thermal storage systems etc.

KEYWORDS: *Thick-walled cylinder, Functionally-graded materials, Transient heat transfer, First order shear deformation theory, Virtual work principle.*

NOTATION

u,ϕ	axial displacements in FSDT
w,ψ	radial displacement in FSDT
E	Young's modulus
ν	Poisson ratio
ρ	FGM density
K	FGM thermal conductivity
α	thermal expansion coefficient
q	heat flux
C	specific heat
$h_{i,o}$	heat flux components
T_∞	reference temperature
T	temperature
$\Delta T(r,t)$	temperature difference
t	time
J	Bessel function of the first kind
Y	Bessel function of the second kind
n_i	inhomogeneity indices
N_x, N_θ, N_z	axial stress resultants
M_x, M_θ, M_z	moment stress resultants
N_{xz}	shear stress resultant
M_{xz}	torsion stress resultant
U	strain energy
U^*	density of strain energy

W	work of external forces
$\bar{r}$	non-dimensional radius
h	thickness of cylinder
L	length of cylinder
R	radius of middle plane
z	distance from middle surface
r	radial coordinate

1. INTRODUCTION

A Functionally Graded Material (FGM) is a non-homogeneous material whose composition is changed continuously from a metal surface to a ceramic surface. This largely circumvents stress concentrations traditionally encountered in other composites since the transition in properties is graded i.e. smooth. Shell structures (e.g. cylindrical, spherical etc) feature in numerous aerospace and mechanical designs including propulsion ducts, rocket chambers, fuel storage tanks etc. Thermal applications of (FGMs) under special conditions were the first aim of designing more effective structures under high-temperature environments including rocket chamber design, nuclear reactors etc. The unique resistance and efficiency of FGMs under different thermal conditions has continued to motivate aerospace and mechanical engineers in further analysis of these robust materials. In this regard, unsteady thermal conduction heat transfer is physically more realistic compared with steady conduction since it encompasses actual conditions witnessed in practical systems (impulsive, shock, pulsed loading etc). Accurate simulation of unsteady conditions is therefore of great relevance to producing viable models of engineering systems and furthermore provides a solid compliment to experimental investigations. An extensive number of studies have been reported on either elastic behavior or steady-state thermo-mechanical analysis of FGM cylindrical shells. However relatively few works have examined *transient* thermo-mechanical loading in FGM shell structures. Hongjun *et al.* [1] presented exact solutions for the multi-layered structure based on Lamé's solution and spread a displacement method for the hollow cylinder with continuously graded properties. Zhifei *et al.* [2] derived a hyper-geometric equation for an *N*-layered elastic hollow cylinder subjected to uniform pressures on the inner and outer surfaces and developed closed-form solutions for a hollow cylinder with continuously graded properties again employing a displacement method. Ghannad and Zamani-Nejad [3] obtained

closed-form solutions for pressurized FGM walled cylindrical shells using the classic method for plane strain and plane stress states. Xin *et al.* [4] presented a solution for a functionally graded thick-walled tube subjected to internal pressure. By using the rule of mixtures and the assumption of a uniform strain field within the two linear elastic constituents, they obtained a hypergeometric differential equation of the radial displacement and thereafter derived the radial displacement and stresses. Ghannad and Zamani Nezhad [5] presented an analytical formulation based on the first order shear deformation theory (FSDT) for axisymmetric thick-walled heterogeneous cylinders under internal and external uniform pressure, assuming isotropic and constant Poisson ratio but with radially varying elastic modulus. Eipackchi *et al.* [6] analyzed the case of a variable thickness cylindrical shell subjected to static non-uniform internal pressure, solving the emerging differential equations with varying coefficients analytically via perturbation theory. Ghannad *et al.* [7] utilized first-order shear deformation theory (FSDT) and the method of matched asymptotic expansions to obtain analytical solutions for deformations and stresses of axisymmetric clamped–clamped thick cylindrical shells with variable thickness composed of functionally graded materials (FGMs) subjected to internal pressure. Belabed *et al.* [8] presented an efficient and simple higher order shear and normal deformation theory for functionally graded material (FGM) plates. They delineated the transverse displacement into bending, shear and thickness stretching parts, thereby reducing the number of unknowns and governing equations and produced extensive solutions using the Navier double expansion technique. Zamaninezhad *et al.* [9] studied theoretically the stress field in a functionally graded rotating thick hollow cylinder with variable thickness and clamped ends under arbitrarily non-uniform pressure on the inner surface, assuming all material properties (except Poisson ratio) to be power law functions of axial coordinate. Arefi and Rahimi [10] presented a thermoelastic analysis of a functionally graded cylinder using first order shear deformation theory (FSDT). Arani *et al.* [11] studied a hollow circular shaft made from functionally graded piezoelectric material (FGPM) rotating about its axis at a constant angular velocity. They considered the case where the shaft is subjected to internal and external pressure, a distributed temperature field due to steady state heat conduction with convective boundary condition, and a constant potential difference between its inner and outer surfaces or combination of these loadings. Keles and Conker [12] focused on non-Fourier hyperbolic heat conduction analysis of heterogeneous hollow cylinders and spheres composed of functionally graded material (FGM) taking all material properties (except thermal relaxation) to vary exponentially across the

thickness. Jabbari *et al.* [13] developed a general solution for one-dimensional steady-state heat transfer in an axisymmetric hollow thick porous FGM cylinder. Temperature was assumed to be a function of the radial direction with general thermal and mechanical boundary-conditions on the inside and outside surfaces. A standard method was used to solve the final nonhomogeneous system of partial differential Navier equations with nonconstant coefficients, using complex Fourier series. Kim and Noda [14] adopted a Green's function approach for analyzing the deflection and the transient temperature distribution in a plate made of functionally graded materials (FGMs). Jabbari *et al.* [15] developed the general analysis of two-dimensional steady-state thermal stresses for a hollow thick cylinder made of functionally graded material, considering the temperature distribution to be a function of radial and circumferential directions. Shao [16] presented solutions for temperature, displacements and thermal/mechanical stresses in a functionally graded circular finite length hollow cylinder under axisymmetric thermal and mechanical loads, by using a multi-layered approach based on the theory of laminated composites. Jabbari *et al*. [17] employed generalized Bessel function to develop exact solutions for steady-state two-dimensional axisymmetric mechanical and thermal stresses for a short hollow cylinder made of functionally graded material, with temperature assumed to be a function of radial and longitudinal coordinates. Malekzadeh *et al.* [18] conducted a detailed transient heat transfer analysis of an FGM hollow cylinder subjected to an axisymmetric distributed heat flux with a moving front boundary on its inner surface using a hybrid finite element-differential quadrature method to discretize the governing equations in the spatial domain. Ootao *et al.* [19] presented an axisymmetric, transient, thermal stress analysis of a hollow cylinder composed of multilayered composite laminates with temperature changes in the radial and axial directions due to axisymmetric heating from the outer and/or the inner surfaces. They applied Fourier cosine transform and Laplace transform methods to the temperature field and the thermoelastic potential function and Love's displacement function approach to the thermoelastic field. Hosseini and Akhlaghi [20] studied the transient thermal stresses in an infinitely long thick hollow cylinder made of a functionally graded material (FGM) under plane strain conditions assuming material properties to be nonlinear with a power law distribution through the thickness and the is supposed. Ghannad and Parhizgar [21] presented solutions for steady state thermo-elastic response of an axisymmetric FGM cylinder subjected to pressure and external heat flux on the inner surface using first order-shear deformation theory (FSDT) and the first order temperature theory. Zidi *et al.* [22]

studied the bending response of functionally graded material (FGM) plate resting on an elastic foundation and subjected to hygro-thermo-mechanical loading, as a simulation of rocket launch pad foundations. They deployed a four variable refined plate theory featuring both a quadratic variation of the transverse shear strains across the thickness and satisfying zero traction boundary conditions on the top and bottom surfaces of the plate without the need for shear correction factors. Raminnia *et al.* [25] investigated the thermo-mechanical nonlinear vibration of a polyethylene (PE) cylindrical shell embedded in an elastic foundation. The shell is reinforced by armchair Carbon nanotubes (CNTs) where characteristics of the equivalent composite being determined using Mori-Tanaka model. Pourasghar *et al.* [26] analyzed the three-dimensional thermo-elastic deformation of cylindrical shells reinforced by singlewalled carbon nanotubes (SWCNTs), subjected to thermal load. The cylindrical shell has been reinforced by Carbon Nanotube (CNT) in the radial direction and the material properties are estimated by the extended rule of mixture. Sepiani *et al.* [27] investigate the free vibration and buckling of a two-layered cylindrical shell made of inner functionally graded (FG) and outer isotropic elastic layer, subjected to combined static and periodic axial forces. Material properties of functionally graded cylindrical shell are considered as temperature dependent and graded in the thickness direction according to a power law distribution in terms of the volume fractions of the constituents. Sepiani et al. [28] investigate the elastic axisymmetric buckling of a thin, simply supported functionally graded (FG) cylindrical shell embedded with an elastic layer under axial compression. The analysis is based on energy method and simplified nonlinear strain-displacement relations for axial compression. Material properties of functionally graded cylindrical shell are considered graded in the thickness direction according to a power-law distribution in terms of the volume fractions of the constituents.

Motivated by extending current studies to consider transient thermal effects, in the current article analytical solutions are developed for thermoelastic behavior of FGM cylinders with power law variation of mechanical and thermal properties under transient heating. The first order shear deformation theory (FSDT) is employed. This is a non-classical theory which contrary to the classical theory includes shear stresses along the cylinder length. The FGM cylindrical shell results are obtained for the case in which two ends of cylinder are mechanically clamped and general heat transfer is present (both convection and conduction). The effects of material distribution on the temperature, displacements and components of stresses through the cylinder are visualized

graphically. The results are found to show good correlation with numerical solutions obtained with a finite element method (FEM).

2. GOVERNING EQUATIONS

The geometrical model of an axisymmetric FGM thick cylindrical shell is depicted in **Fig. 1**. In first shear deformation theory (FSDT) according to **Fig**.1 and Mirsky-Hermann assumption [23] the interspace of each point of the shell from the symmetry axis i.e. radial coordinate (*r*) is equal to summation of middle plane's radius (*R*) and interspace of that point from this middle plane (*z*). The displacement vector and first order displacement field according to Mirsky-Hermann [23] assumption with considering the vertical transverse strains may be defined generally as below:

$$\vec{U} = \overrightarrow{U_0} + \overrightarrow{U_1} z + \overrightarrow{U_2} z^2 + \cdots = \sum_{m=0}^{\infty} \overrightarrow{U_m} z^m \tag{1}$$

$$\begin{Bmatrix} U_x \\ U_z \end{Bmatrix} = \begin{Bmatrix} \phi_0 \\ \psi_0 \end{Bmatrix} + \begin{Bmatrix} \phi_1 \\ \psi_1 \end{Bmatrix} z \tag{2}$$

The strain tensor for small deformations in vector form and the strain field according to kinematic relations for axisymmetric conditions are [23]:

$$\tilde{\varepsilon} = \frac{1}{2}\left[(\vec{\nabla}\vec{U}) + (\vec{\nabla}\vec{U})^T\right] \tag{3}$$

$$\begin{cases} \varepsilon_x = \dfrac{\partial U_x}{\partial x} = \acute{\phi}_0 + \acute{\phi}_1 z \\ \varepsilon_\theta = \dfrac{U_z}{R} = \dfrac{1}{R+z}(\psi_0 + \psi_1 z) \\ \varepsilon_z = \dfrac{\partial U_z}{\partial z} = \psi_1 \\ \gamma_{xz} = \dfrac{\partial U_X}{\partial Z} + \dfrac{\partial U_z}{\partial x} = \left(\phi_1 + \acute{\psi}_0\right) + \acute{\psi}_1 \end{cases} \tag{4}$$

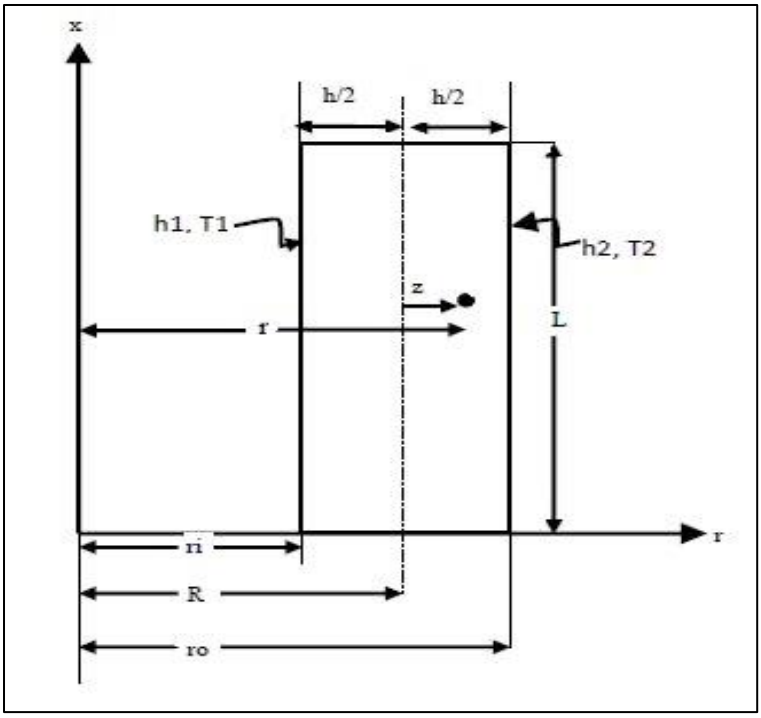

Fig. 1 Section of thick-walled cylinder under transient heating

The components of the stress resultants are [23]:

$$\{N_x, N_\theta, N_z, N_{xz}\} = \int \left\{\sigma_x, \frac{\sigma_\theta}{1+{}^{z}/_{R}}, \sigma_z, \tau_{xz}\right\}\left(1+\frac{z}{R}\right)dz$$
$$\{M_x, M_\theta, M_z, M_{xz}\} = \int \left\{\sigma_x, \frac{\sigma_\theta}{1+{}^{z}/_{R}}, \sigma_z, \tau_{xz}\right\}(1+\frac{z}{R})z\,dz \quad (5)$$

2-1 Thermoelastic analysis of heterogeneous cylinders

According to the principle of virtual work, the variation of strain energy is equal to the work done by external forces.

$$\delta U = \delta W \quad (6)$$

With consideration of the constitutive equation for heterogeneous and isotropic materials and thermal strains, the stresses in terms of strains take the form below [21]:

$$\begin{cases} \sigma_i = \lambda E(r)\left[(1-\upsilon)\varepsilon_i + \upsilon\left(\varepsilon_j+\varepsilon_k\right) - \alpha(r)(1+\upsilon)\Delta T(r,t)\right] \\ \tau_{xz} = \dfrac{1-2\upsilon}{2}\lambda E\gamma_{xz} \qquad\qquad i \neq j \neq k \\ \lambda = \dfrac{1}{(1+\upsilon)(1-2\upsilon)} \end{cases} \quad (7)$$

By defining the strain energy as below and substituting Eqn. (7) into (8), strain energy in terms of strains is obtained. [21]

$$\begin{cases} U = \iiint_V U^* dV \,, dV = r dr d\theta dx = (R+z) dx d\theta dz \\ U^* = \frac{1}{2}(\varepsilon_x \boldsymbol{\sigma_x} + \varepsilon_\theta \boldsymbol{\sigma_\theta} + \varepsilon_z \boldsymbol{\sigma_z} + \tau_{xz}\gamma_{xz}) \\ U = \frac{1}{2}E(r)\lambda\big[(1-\upsilon)\big(\varepsilon_x^2 + \varepsilon_\theta^2 + \varepsilon_x^2\big) + 2\upsilon(\varepsilon_x\varepsilon_z + \varepsilon_x\varepsilon_\theta + \varepsilon_\theta\varepsilon_z) \\ \quad + \frac{1-2\upsilon}{2}\gamma_{xz}^2 - a(r)\Delta T(r,t)(1+\upsilon)(\varepsilon_x + \varepsilon_\theta + \varepsilon_z)\big] \end{cases} \tag{8}$$

In the absence of external forces, $\delta W = 0$. After calculating the energy integral and using the virtual work principle, the equilibrium equations for the FGM cylindrical shell under transient heat transfer in terms of stress resultants and associated boundary conditions emerge:

$$\begin{cases} RN_x^{'} = 0 \\ RM_x^{'} - RN_{xz} = 0 \\ RN_{xz}^{'} - N_\theta = 0 \\ RM_{xz}^{'} - M_\theta - RN_z = 0 \end{cases} \tag{9}$$

$$R[N_x\delta\phi_0 + M_x\delta\phi_1 + N_{xz}\delta\psi_0 + M_{xz}\delta\psi_1]_0^L = 0 \tag{10}$$

2-2 Distribution of mechanical and thermal properties

In the present analysis, the mechanical and thermal properties of the FGM varying according to a power law distribution. Young modulus (E), density (ρ), thermal expansion coefficient (α), thermal conductivity (K) and specific heat capacity (C) vary with radial coordinate of the cylinder as given below: [5]

$$E = E_i\left(\frac{r+z}{r_i}\right)^{n_4} \tag{11}$$

$$\rho = \rho_i\left(\frac{r+z}{r_i}\right)^{n_2} \tag{12}$$

$$\alpha = \alpha_i\left(\frac{r+z}{r_i}\right)^{n_5} \tag{13}$$

$$K = K_i\left(\frac{r+z}{r_i}\right)^{n_1} \tag{14}$$

$$C = C_i\left(\frac{r+z}{r_i}\right)^{n_3} \tag{15}$$

where E_i ، α_i ، K_i ، C_i ، ρ_i are properties of the cylinder inner surface and n_i (i=1-5) are the FGM material heterogeneous constants. **Fig. 2** shows the power-law variation in property variation used in the study.

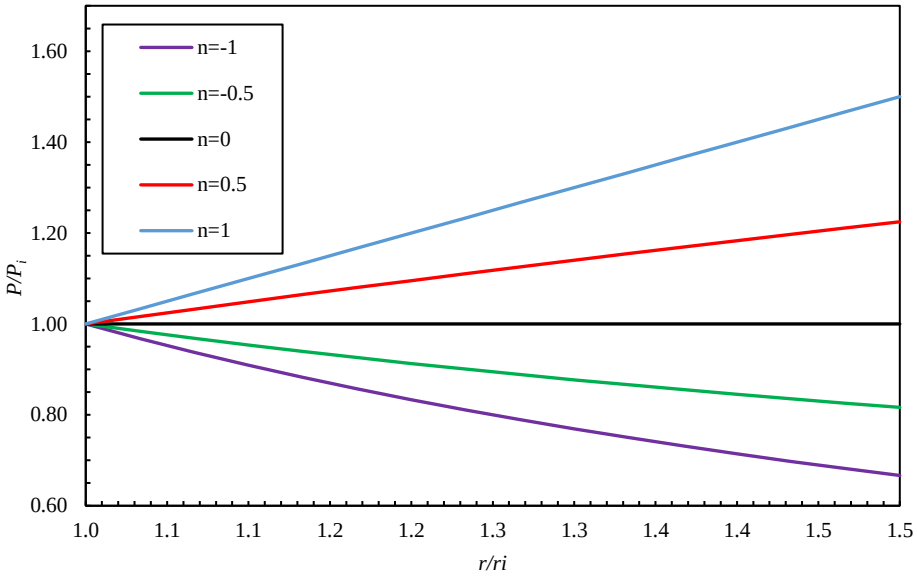

Fig. 2 Non-dimensional distribution of arbitrary properties with dimensionless radial coordinate

2-3 Analytical solution of unsteady heat transfer of FGM cylinder [24]

The equation for unsteady heat transfer in a thick walled FGM cylinder in the absence of heat source terms is:

$$\rho c \frac{\partial T}{\partial t} = \frac{1}{r}\frac{\partial}{\partial r}\left(Kr\frac{\partial T}{\partial r}\right) \tag{16}$$

The relevant thermal boundary and initial conditions (B.C. and I.C.) employed in the current study are formulated in general form where both conduction and convection are considered:

$$\text{B. C.}\begin{cases} c_{11}T(r_i,t) + c_{12}\dfrac{\partial T}{\partial r}(r_i,t) = g_1 \\ c_{21}T(r_0,t) + c_{22}\dfrac{\partial T}{\partial r}(r_0,t) = g_2 \end{cases} \tag{17}$$

$$\text{I. C.}\ \ \{T(r,0) = T_i(r)$$

Here C_{ij} and g_i (i,j=1,2) are constants.

The method of separation of variables is used for solving the unsteady heat transfer equation. It is therefore judicious to change the heterogeneous boundary conditions to homogeneous ones:

$$T(r,t) = T_h(r,t) + T_s(r) \tag{18}$$

By substituting Eqn. (18) into Eqn. (16) the homogeneous boundary conditions are separated from the heterogeneous ones.

$$\rho c \frac{\partial T_h(r,t)}{\partial t} = \frac{1}{r}\frac{\partial}{\partial r}\left(Kr\left(\frac{\partial T_h(r,t)}{\partial r} + \frac{\partial T_s(r)}{\partial r}\right)\right) \tag{19}$$

$$\begin{cases} \rho c \dfrac{\partial T_h(r,t)}{\partial t} = k\dfrac{\partial^2 T_h(r,t)}{\partial r^2} + \left(\dfrac{\partial k}{\partial r} + \dfrac{k}{r}\right)\dfrac{\partial T_h(r,t)}{\partial r} \\ \dfrac{1}{r}\dfrac{\partial}{\partial r}\left(Kr\dfrac{\partial T_s(r)}{\partial r}\right) = 0 \end{cases} \tag{20}$$

$$\begin{cases} c_{11}T_s(r_i) + c_{12}\dfrac{\partial T_s}{\partial r}(r_i) = g_1 \\ c_{21}T_s(r_0) + c_{22}\dfrac{\partial T_s}{\partial r}(r_0) = g_2 \end{cases} \tag{21}$$

$$\begin{cases} c_{11}T_h(r_i,t) + c_{12}\dfrac{\partial T_h}{\partial r}(r_i,t) = 0 \\ c_{21}T_h(r_0,t) + c_{12}\dfrac{\partial T_h}{\partial r}(r_0,t) = 0 \end{cases} \tag{22}$$

$$T_h(r,0) = T_i(r) - T_s(r)$$

After double integration of the second part of Eqn. (20), T_s is investigated where by substituting the boundary condition of Eqn. (21), two integration constants emerge.

$$T_s(r) = C_1 Ln(r) + C_2$$

$$\mathrm{C_1} = \frac{\mathrm{g_1 c_{21} - g_2 c_{11}}}{\mathrm{c_{11}c_{21}r_1^{-n_1} - r_0^{-n_1} + n_1 c_{22}c_{11}r_0^{-n_1-1} - c_{12}c_{21}r_i^{-n_1-1}}}$$

$$\mathrm{C_2} = \frac{\mathrm{g_1 - c_1 c_{11} r_i^{-n_1} - c_{12} n_1 r_i^{-n_1-1}}}{\mathrm{c_{11}}} \tag{23}$$

For solving the first part of Eqn. (20) the method of separation of variables is used.

$$T_h(r,t) = f(r)g(t) \tag{24}$$

$$\frac{1}{g(t)}\frac{\partial g(t)}{\partial t} = \frac{1}{\rho c}\left(\frac{k}{f(r)}\frac{\partial^2 f(r)}{\partial r^2} + \left(\frac{\partial k}{\partial r} + \frac{k}{r}\right)\frac{1}{f(r)}\frac{\partial f(r)}{\partial r}\right) \tag{25}$$

$$\begin{cases} K\dfrac{\partial^2 f(r)}{\partial r^2}+\left(\dfrac{\partial k}{\partial r}+\dfrac{k}{r}\right)\dfrac{\partial f(r)}{\partial r}+S^2\rho c f(r)=0 \\ \dfrac{\partial g(t)}{\partial t}+S^2 g(t)=0 \end{cases} \tag{26}$$

The solution for $T_h(r,t)$ is obtained as:

$$T_h(r,t) := r^{-p}\left[d_1 J_{\frac{q}{x}}(0)+d_2 Y_{\frac{q}{x}}(0)\right]+\sum_{n=1}^{\infty} r^{-p}\left[A_n J_{\frac{q}{x}}\left(s'^{r^x}\right)+B_n Y_{\frac{q}{x}}\left(s'^{r^x}\right)\right]e^{-s_n^2 t} \tag{27}$$

where:

$$q=\sqrt{p^2-\beta^2}=p \tag{28}$$

$$\frac{\alpha}{x}=s' \tag{29}$$

$$p=q=\frac{n_1}{2} \tag{30}$$

$$x=\frac{2-n_1+n_2+n_3}{2} \tag{31}$$

$$s_n'=\frac{1}{x}\sqrt{\frac{r_1^{n_1-n_2-n_3}s_n^2\rho_1 c_1}{k_1}} \tag{32}$$

After substituting the boundary condition of Eqn. (22) the *characteristic equation* in terms of Bessel functions is obtained:

$$c_{22}xs_n'r_0^{x-1}f_{\frac{q}{x}+1}(s_n',r_0^x)-c_{21}f_{\frac{q}{x}}(s_n',r_0^x)=0 \tag{33}$$

$$\begin{aligned} f_{\frac{q}{x}}(s_n',r^x) = {} & J_{\frac{q}{x}}(s_n',r^x)\left[c_{11}Y_{\frac{q}{x}}(s_n'r_i^x)-\ c_{12}s_n'xr_i^{x-1}Y_{\frac{q}{x}+1}(s_n'r_i^x)\right] \\ & -\ Y_{\frac{q}{x}}s_n'r^x\left[c_{11}J_{\frac{q}{x}}(s_n'r_i^x)-\ c_{12}s_n'xr_i^{x-1}J_{\frac{q}{x}+1}(s_n'r_i^x)\right] \end{aligned} \tag{34}$$

$$T_h(r,t)=\sum_{n=1}^{\infty}A_n r^{-p}\,f_{\frac{q}{x}}(s_n',r^x)e^{-s_n^2 t} \tag{35}$$

Here A_n is a constant and can be derived by Sturm-Liouville theory after substituting the initial condition of Eqn. (22).

$$A_n=\frac{\int_{R_i}^{R_o} r^{p+1}T_h(r,0)f_{\frac{q}{x}}(s_n',r^x)dr}{\int_{R_i}^{R_o} r^{p+1}f_{\frac{q}{x}}{}^2(s_n',r^x)dr} \tag{36}$$

Therefore, the unsteady temperature distribution in the FGM cylindrical shell may be obtained.

$$T(r,t) = \sum_{n=1}^{\infty} A_n r^{-p} f_{\underline{\underline{q}}}(s_n', r^x)\, e^{-s_n^2 t} + c_1 r^{-n_1} + c_2 \qquad (37)$$
$$\Delta T(z,t) = T(z,t) - T_\infty$$

2-4 Thermoelastic analysis of FGM cylinder under unsteady general heating

Eqn. (9) constitutes a set of differential equations which may be written in terms of displacement by using Eqns. (5) and (4). This leads to a system of 4 differential equations. These equations are heterogeneous and linear and have constant coefficients.

$$[A]\frac{d^2}{dx^2}\{y\} + [B]\frac{d}{dx}\{y\} + [C]\{y\} = \{F\} \qquad (38)$$

$$\{y\} = \{\phi_0\ \phi_1\ \psi_0\ \psi_1\}^T \qquad (39)$$

where $\{F\}$ is the external "force" vector which in this study is the heterogeneous part of the equations and include unsteady heating.

$$\{F\} = \begin{Bmatrix} 0 \\ 0 \\ -\alpha_i \int_{-\frac{h}{2}}^{\frac{h}{2}} \left(\frac{R+z}{r_i}\right)^{2n} \Delta T(z,t)(1+v)dz \\ -\alpha_i \int_{-\frac{h}{2}}^{\frac{h}{2}} \left(\frac{R+z}{r_i}\right)^{2n} \Delta T(z,t)(1+v)(R+2z)dz \end{Bmatrix} \qquad (40)$$

In equation (38) $[A]_{4\times4}$and $[C]_{4\times4}$ are axisymmetric matrices and $[B]_{4\times4}$ is an anti-symmetric matrix where the associated elements are listed in **Appendix A**. Proceeding with the analysis, next $\{y\} = \{\xi\}e^{mx}$ is substituted in the left-hand side of Eqn. (38) to obtain the general solution:

$$e^{mx}[m^2A_1 + mA_2 + A_3]\{\xi\} = \{0\} \qquad (41)$$

$$|m^2A_1 + mA_2 + A_3| = 0 \qquad (42)$$

The Eigenvalue of Eq. (42) contain two pairs of conjugate roots and a pair of real roots. By substituting the Eigenvalues in Eqn. (38), the corresponding Eigenvectors can be obtained. The general and particular solutions are:

$$\{y\}_g = \sum_{i=1}^{6} C_i \{\xi\}_i e^{m_i x} \tag{43}$$

$$[C]\{y\} = \{F\} \Rightarrow \{y\} = [C]^{-1}\{F\} \tag{44}$$

The boundary conditions are as stipulated in Eqn. (10) and therefore all of the unknowns are obtainable.

3. RESULTS AND DISCUSSION

To extract some results, the case where both ends of the FGM cylinder shell are clamped is considered. According to Eq. (10) therefore:

$$\begin{cases} x = 0 \Rightarrow \phi_0 = 0, \phi_1 = 0, \psi_1 = 0, \psi_1 = 0 \\ x = L \Rightarrow \phi_0 = 0, \phi_1 = 0, \psi_1 = 0, \psi_1 = 0 \end{cases} \tag{45}$$

In order to compare the analytical results with numerical solutions based on a finite element method (FEM), parameter values for the case studied are as prescribed in **Table 1**.

Table 1. Case study values

Quantity	**value**
Inner radius	$r_i = 0.4m$
Outer radius	$r_o = 0.6m$
Length	$L = 8m$
Young modulus	$E_i = 200GPa$
Poisson ratio	$\nu = 0.3$
density	$\rho_i = 7854\, kg/m^3$
Expansion coefficient	$\alpha_i = 12(10^{-6})\, 1/°K$
Specific heat	$c_i = 434\, j/kg°K$
Thermal conductivity	$k_i = 60.5\, W/m°K$

Inner heat transfer coefficient	$C_{11} = 6W\ /m^2K$
Outer heat transfer coefficient	$C_{21} = 25W/m^2K$
Inner fluid temperature	$T_{\infty 1} = 280.15°K$
Outer fluid temperature	$T_{\infty 2} = 285.15°K$

Graphical results based on the prescribed data are visualized in **Figs. 2-16**. Fig. 3 shows the temperature distribution in different times. At finite time values there is generally a sigmoidal profile in radial temperature. With increasing *t* value the temperature at low values of radial coordinate are increased whereas those at higher values of radial coordinate are reduced. However, after a long time elapse (*t*= infinity) the temperature becomes constant and corresponds to steady conditions.

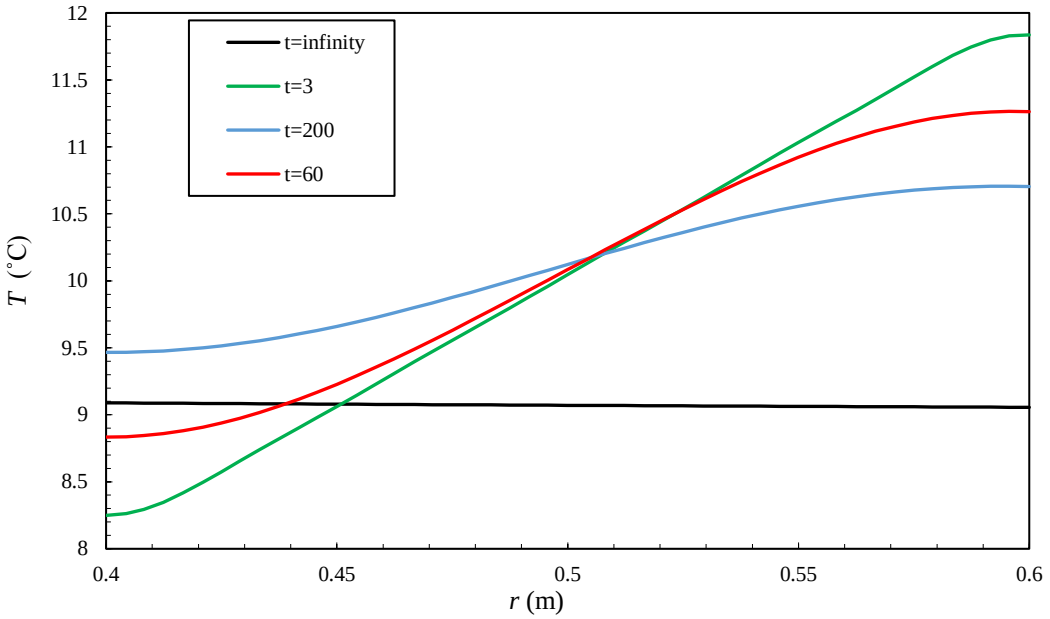

Fig. 3 Radial temperature distribution for different times

Figs. 4-5 illustrate the radial displacement distribution in the homogenous FGM cylinder (i.e. for *n*=0) at different times. A weak depletion in radial displacements is observed for all time values with a progressive increase in dimensionless radial coordinate. However, for higher *t* value (*t* = 40) the magnitude of radial displacement is significantly greater than at lower time values (t=10,20,30). The impact of increasing time is therefore to enhance radial displacements.

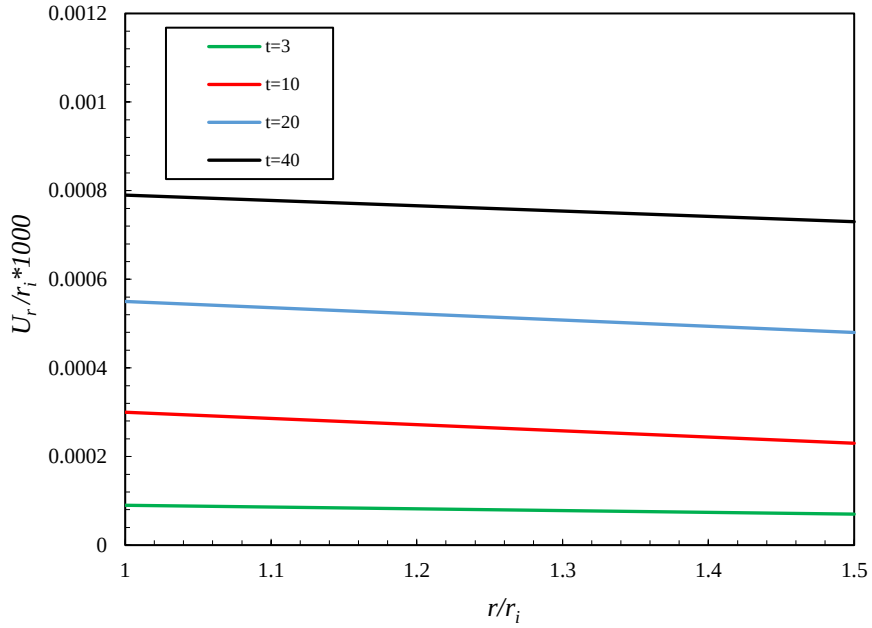

Fig. 4 Non-dimensional radial displacement distribution of homogeneous cylinder at x=L/2

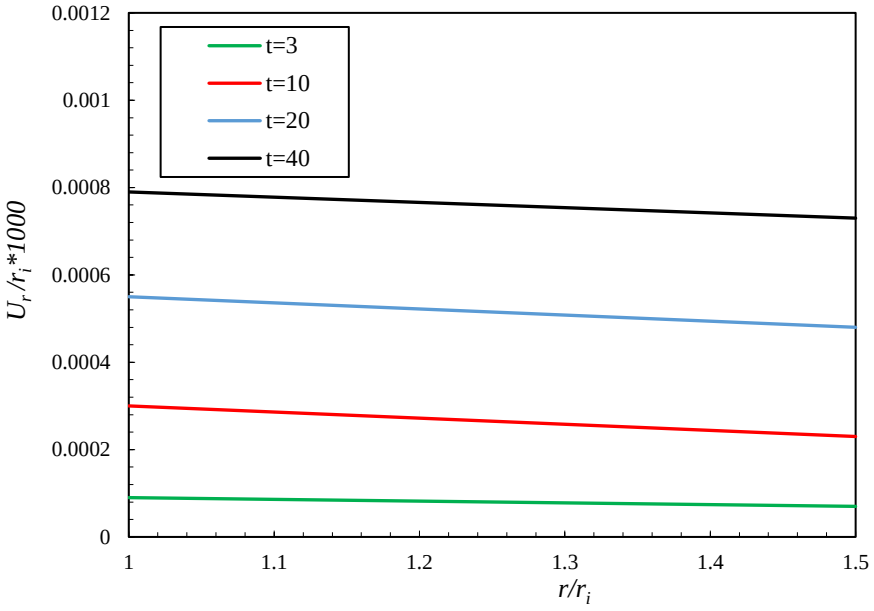

Fig. 5 Radial displacement distribution of heterogeneous FGM cylinder (*n>0*) at x=L/2.

A similar response is computed in Fig. 5 for the heterogeneous FGM cylinder (*n>0*) case i.e. radial displacements are also generally boosted with elapse in time. Again, a linear decay in radial displacement is computed with increasing dimensionless radial coordinate.

Fig. 6 illustrates the evolution in non-dimensional hoop stress for the heterogeneous cylinder for different *n* (heterogeneous constants) at *t = 40 s*. The case of a homogenous cylinder corresponds to *n*=0. The figure shows that at a point near the middle plane the hoop stresses converge to the same value, i.e. at this location the hoop stresses are independent of material properties. The deviation of *n*=0 from the other cases ($n \neq 0$) is due to the derivative errors associated with the FSDT formulation. For negative values of *n* the hoop stress is maximized at the cylinder inner surface ($r/r_i=0$) whereas it is minimized at the outer periphery. The reverse behavior is computed for increasingly positive values of n i.e. the hoop stress is minimized at the cylinder inner surface ($r/r_i=0$) whereas it is maximized at the outer periphery

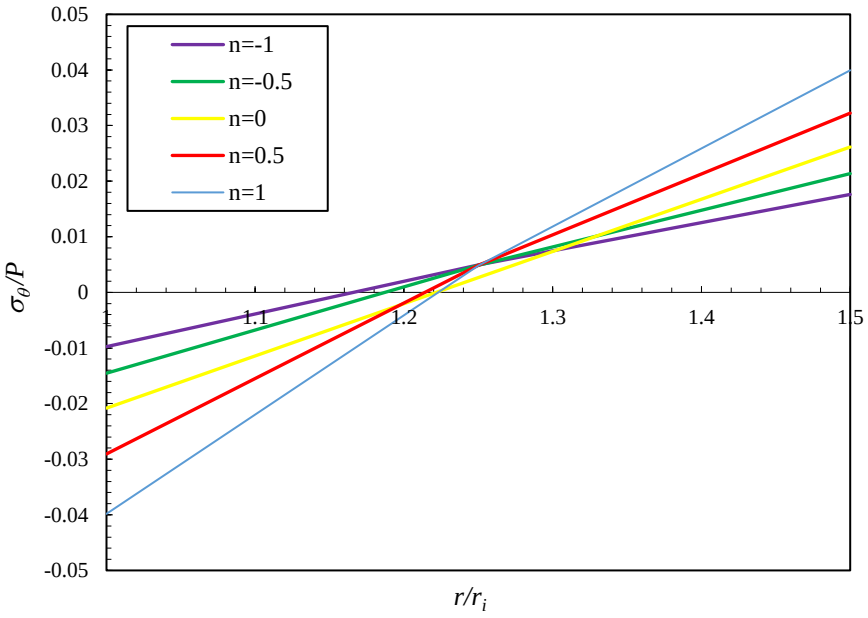

Fig. 6 Hoop stress distribution of FGM cylinder at x=L/2, t=40 s

Figs. 7-8 show the effects of boundary conditions on radial and axial displacements of the cylinder. Fig. 7 indicates an abrupt change in radial displacement near the ends of cylinder which is due to the end constraint considerations. A plateau-like distribution is however observed for radial displacement for the majority of the cylinder length and magnitudes do not change sign i.e. consistently positive radial displacements are computed along the length of the cylinder.

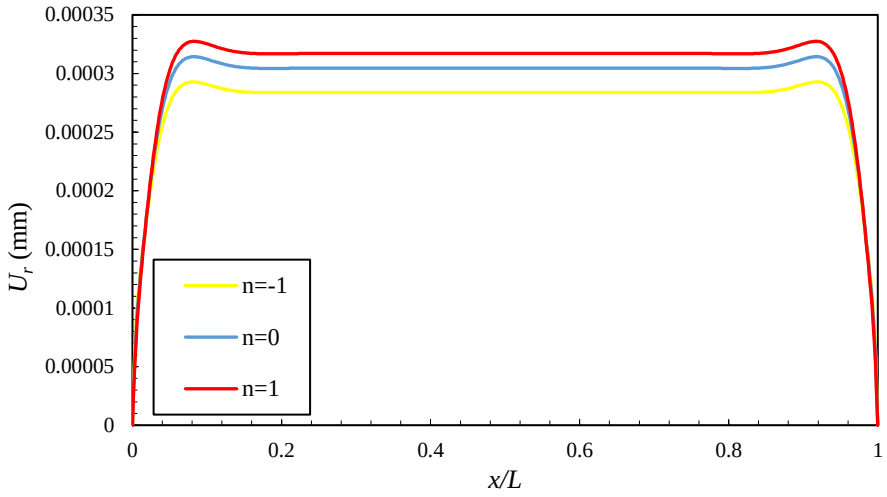

Fig. 7 Radial displacement distribution at *z=0, t=40 s*

For negative value of the heterogeneous constant, *n*, significantly lower magnitudes of radial displacement are computed compared with those for a positive value of the heterogeneous constant *n*. The case for a homogenous cylinder ($n = 0$) falls between the other two cases. Fig. 7 shows a significantly different distribution in axial displacements. Although sharp elevations and depletions in axial displacement arise near the start and end of the cylinder, the profiles are generally linear decays from lower axial coordinate values to the opposite end of the cylinder. Higher values of axial displacement are computed for $n = 1$ compared with $n = -1$ with the homogenous case ($n = 0$) again falling between these other two cases.

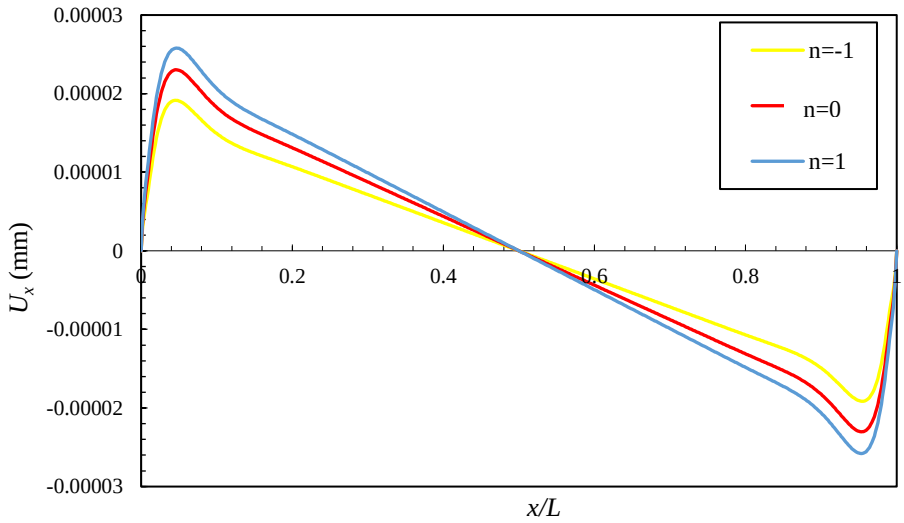

Fig. 8 Axial displacement distribution at *z=0, t=40s*

Figs. 9-11 depict the distributions for hoop and shear stresses for different values of *n*. Fig. 9 shows that for all values of *n* there is an increase in hoop stress at the start of the cylinder whereas there is a significant decrease at the end of the cylinder. In the intermittent region a plateau-like distribution is computed. With increasing *n* values there is a substantial reduction in hoop stress. According to fig. 10 the shear stress values are considerable at the boundaries whereas they vanish for the majority of the cylinder length. Increasing *n* values exert no tangible influence on shear stress and this is attributable to the limitations of the first order shear deformation theory (FSDT). To capture modifications in shear stress with heterogenous constant (n) a *higher* order shear deformation theory is worth exploring.

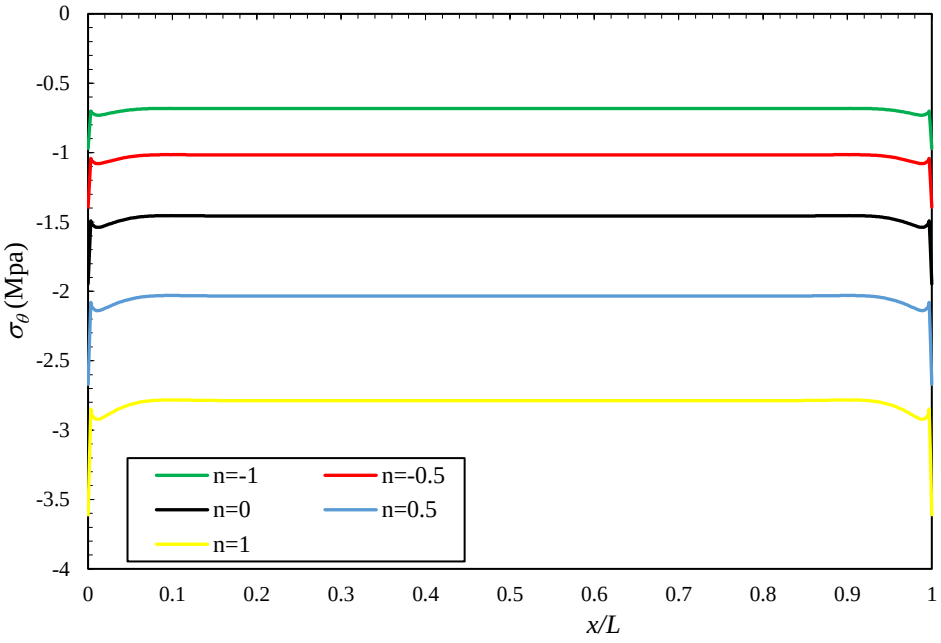

Fig. 9 Hoop stress distribution at z=-h/2, t=40 s

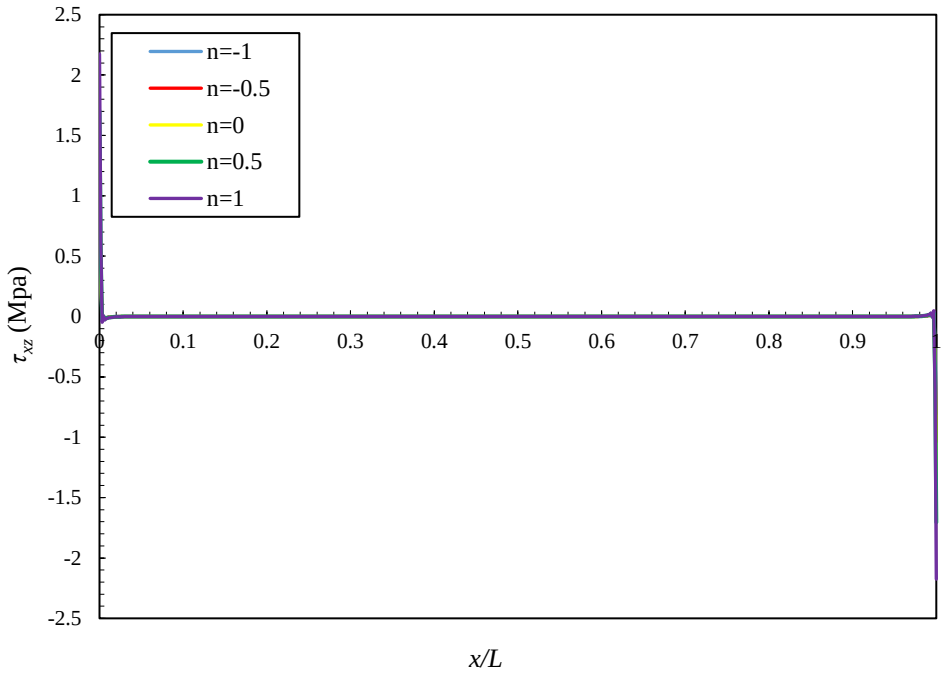

Fig. 10 Shear stress distribution at z=0, t=40 s

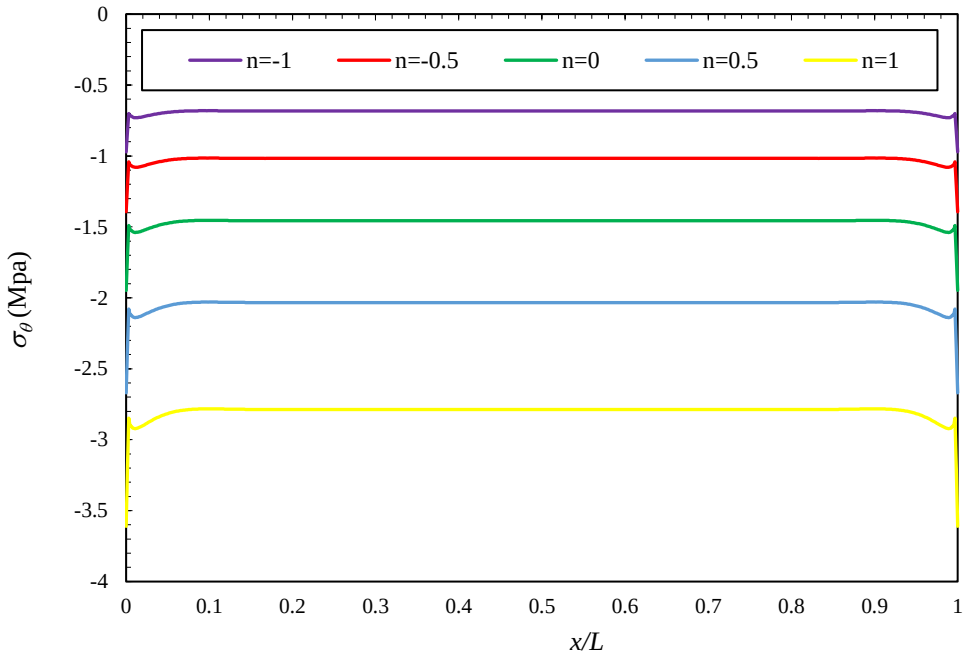

Fig. 11 Comparison of hoop stress distribution in different layers at t=40 s for n=1

Fig. 11 shows the hoop stresses values for different layer of cylinder i.e. not at the z=h/2 location. A similar distribution is computed as in Fig. 9. Hoop stresses are elevated with negative values of n and decreased with positive values.

Fig. 12 indicates the variation of radial displacement with time for different values of heterogenous constant (*n*). It is evident that radial displacement increases with the elapse of time and the profiles are generally linear in nature. Positive values of heterogenous constant (*n*) invariably enhance radial displacement magnitudes whereas the contrary behavior is induced with negative values of heterogenous constant (*n*).

Fig. 13 indicates that the hoop stress values are decreased with progress in time. Higher (i.e. more positive) values are associated with negative heterogenous constant (*n*=-1) whereas the lowest (most negative) values correspond to positive heterogenous constant (*n*=1). In all cases the profiles are monotonic decays from a maximum hoop stress at *t*=0 to a minimum hoop stress at maximum time value (*t*=40s). Finally, in Fig. 14 the transient distributions of radial displacement are plotted for the heterogenous FGM cylinder (*n*=1) and the homogenous cylinder (*n*=0). Maximum radial displacements are observed at the start of the cylinder and the end of the cylinder. Higher values of radial displacement are computed at higher time values and the heterogenous case achieves higher magnitudes than the homogenous case.

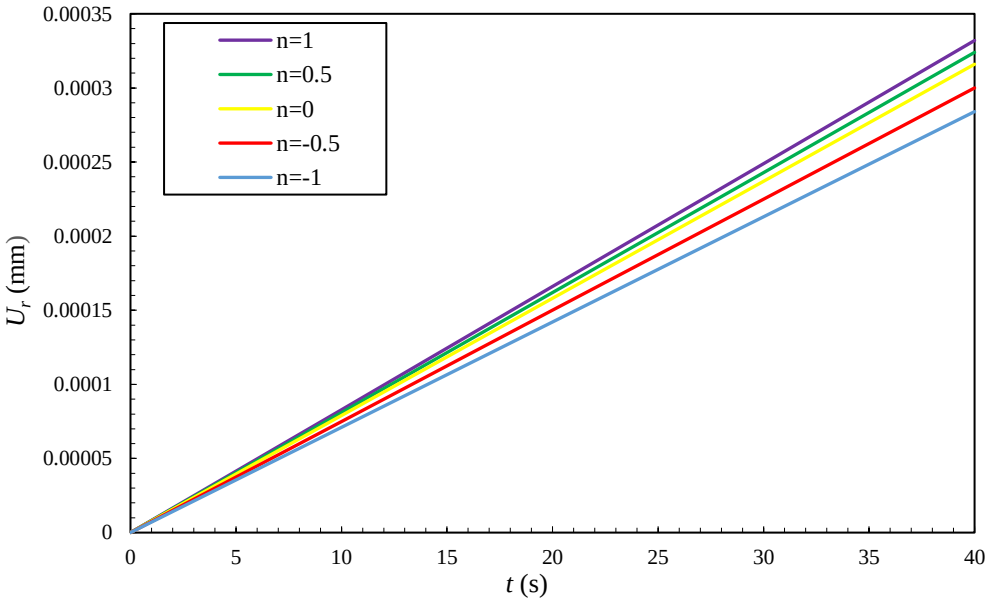

Fig. 12 Radial displacement distribution versus time at z=0, t=40 s

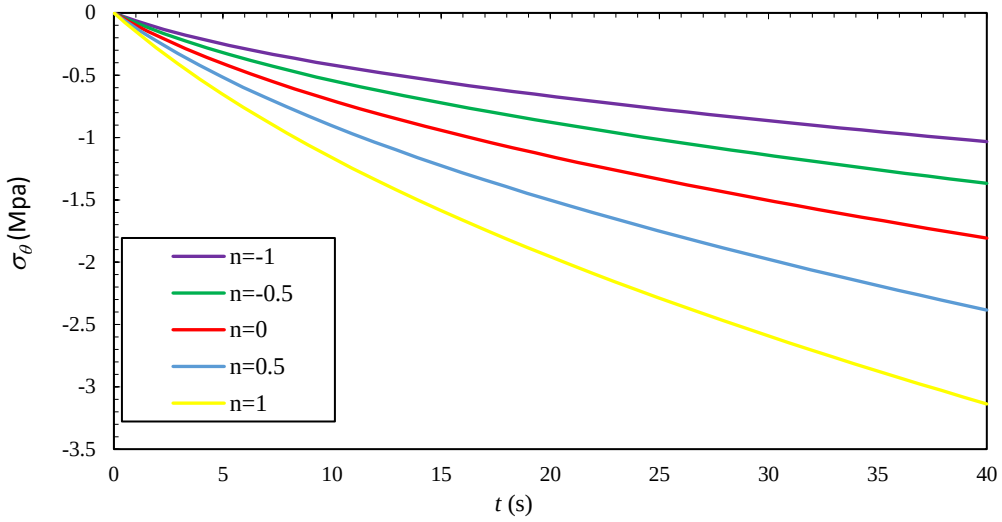

Fig. 13 Hoop stress distribution versus time at x=L/2, z=-h/2

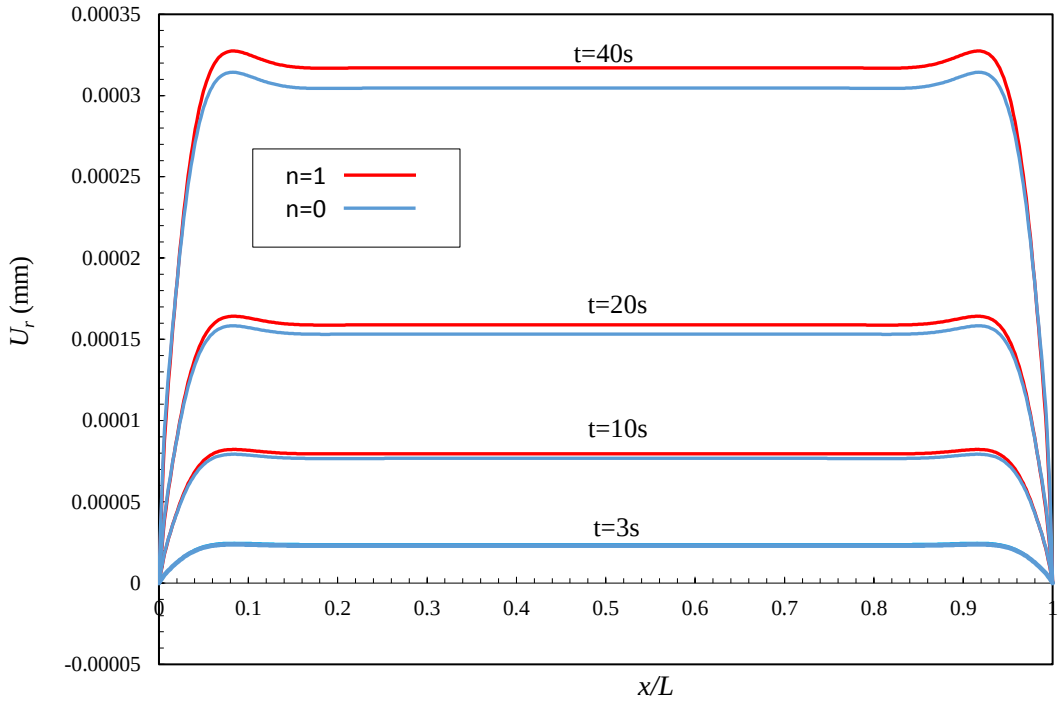

Fig. 14 Comparison of radial displacement at different times and different heterogeneous constants (n) at z=0

For validation of the results numerical solutions have also been obtained with a Finite Element Method (FEM). Details of the solution are omitted for brevity. **Figs. 15-16** and Table 2 illustrate

the differences between the numerical and analytical solutions for temperature distribution with radial coordinate, radial displacement and Hoop stress with axial coordinate. The closed-form solutions based on FSDT achieve reasonable agreement with FEM solutions. For more accuracy a higher order shear deformation theory is suggested.

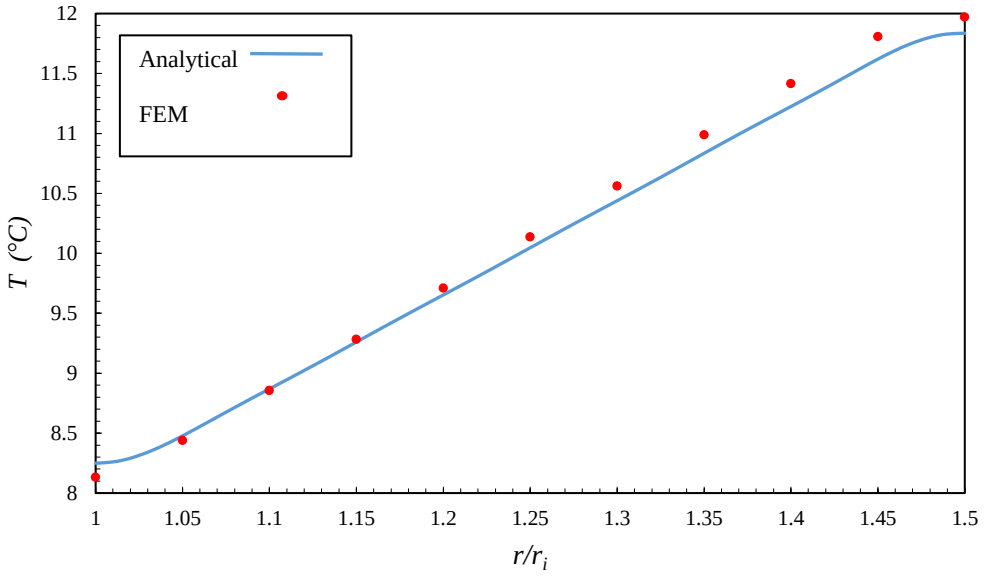

Fig. 15 Temperature distribution at t=3s, n=0 - results of FSDT and FEM

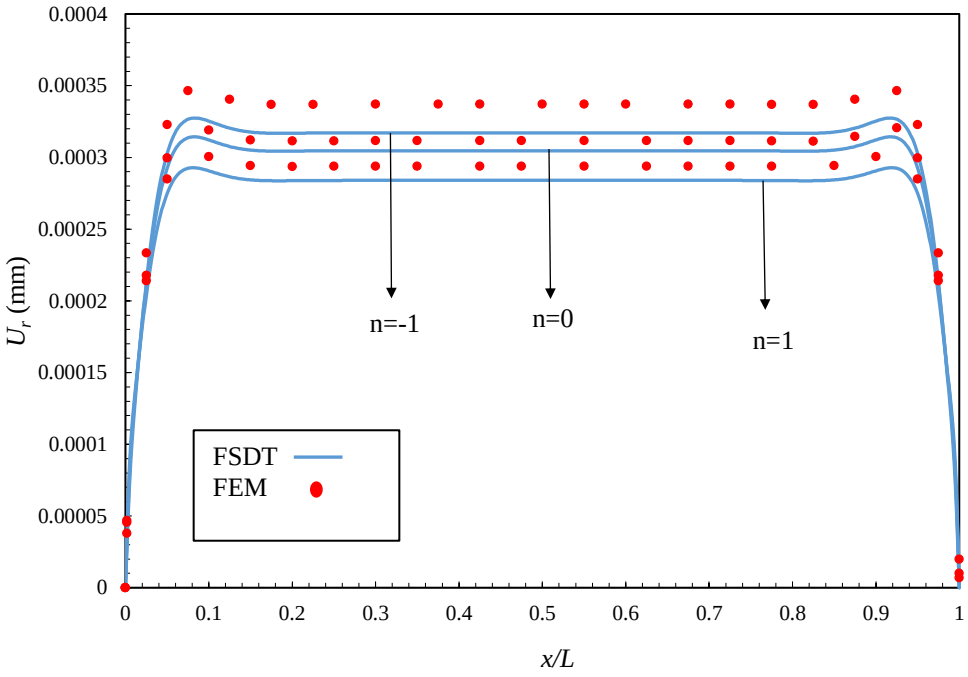

Fig. 16 Radial displacement at z=0, t=40 s - results of FSDT and FEM

Table 2. Hoop stress according to FSDT and FEM

σ_θ [Mpa]	r=R(Middle Surface)		r=ri	
	FSDT	**FEM**	**FSDT**	**FEM**
n=-1	0.344	0.435	-0.682	0.227
n=-0.5	0.343	0.43	-1.017	0.204
n=0	0.324	0.421	-1.457	0.198
n=0.5	0.3405	0.387	-2.033	1.22
n=1	0.339	0.383	-2.787	1.451

By considering the inner pressure of 70MPa, $T_i(r) = 20r$ and constant temperature at inner and outer surface (According to the [24] conditions) the results of current work can be valid with Afshin et.al [24] paper. Their method was based on Plane strain theory (PET) that the shear strain and shear stress weren't observed.

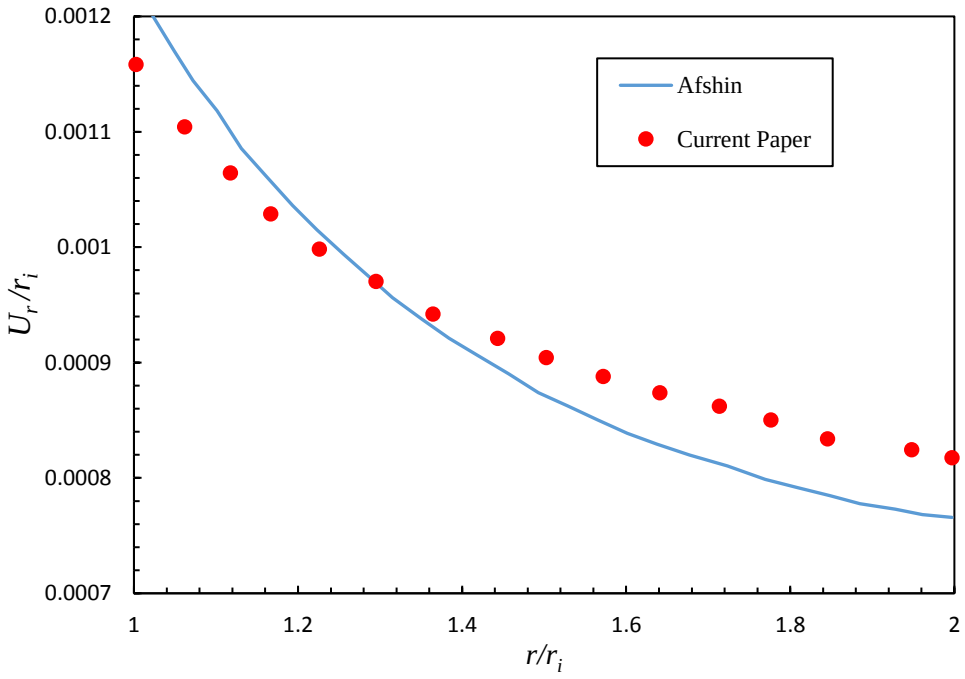

Fig. 17 Validation of obtained results with respect to other work at t=5 s.

4. CONCLUSIONS

This paper presents a mathematical study of the unsteady thermoelastic response of an axisymmetric FGM cylinder which is subjected to transient thermal loading conditions. Closed-form solutions are developed for the unsteady heat transfer and equilibrium equations by using separation of variables and energy methods. The important findings may be summarized as follows:

(1) The existing results from the literature based on plain strain theory are extended using first order shear deformation theory to successfully simulate length and shear stress effects.

(2) The analytical approach developed is suitable for modelling the end effects of the cylinder, and the unsteady thermoelastic model provides a more accurate simulation for shear stress and heat transfer.

(3) The shear stresses are significant at regions near to the ends of the finite cylinder and approximately equal to zero at the middle-plane of the cylinder.

(4) Temperature is increased with the passage of time until the steady state scenario is attained.

(5) Material inhomogeneity (as simulated via a heterogenous constant for the FGM) plays a significant role in modifying both the mechanical and thermal behavior.

(6) Radial and axial displacement values are increased when the heterogenous (power law index) constant is increased.

(7) An optimum value for *n* can be selected which is useful for designers.

(8) For each value of *n* the maximum hoop or radial stress is increased at one edge of the cylinder and decreased at the opposite end.

The present study may be extended to incorporate heat source (generation and absorption) and thickness stretching effects [22] and these may be considered in the near future.

APPENDIX A

$$A_{11} = R(1-v)\int_{-h/2}^{h/2}\left(\frac{R+z}{r_i}\right)^n\left(1+\frac{z}{R}\right)dz$$

$$A_{12} = R(1-v)\int_{-h/2}^{h/2}\left(\frac{R+z}{r_i}\right)^n\left(1+\frac{z}{R}\right)zdz = A_{21}$$

$$A_{22} = R(1-v)\int_{-h/2}^{h/2}\left(\frac{R+z}{r_i}\right)^n\left(1+\frac{z}{R}\right)z^2dz$$

$$A_{33} = R\mu(1-v)\int_{-h/2}^{h/2}\left(\frac{R+z}{r_i}\right)^n\left(1+\frac{z}{R}\right)dz$$

$$A_{34} = R\mu(1-v)\int_{-h/2}^{h/2}\left(\frac{R+z}{r_i}\right)^n\left(1+\frac{z}{R}\right)zdz = A_{43}$$

$$A_{44} = R\mu(1-v)\int_{-h/2}^{h/2}\left(\frac{R+z}{r_i}\right)^n\left(1+\frac{z}{R}\right)z^2dz$$

$$A_{13} = A_{14} = A_{23} = A_{24} = A_{31} = A_{32} = A_{41} = A_{42} = 0$$

$$B_{13} = v\int_{-h/2}^{h/2}\left(\frac{R+z}{r_i}\right)^n dz = -B_{31}$$

$$B_{14} = v\int_{-\frac{h}{2}}^{\frac{h}{2}}\left(\frac{R+z}{r_i}\right)^n (R+2z)dz = -B_{41}$$

$$B_{23} = \int_{-h/2}^{h/2}\left(\frac{R+z}{r_i}\right)^n [(v-\mu)z - R\mu]dz = -B_{32}$$

$$B_{24} = \int_{-\frac{h}{2}}^{\frac{h}{2}}\left(\frac{R+z}{r_i}\right)^n [R(v-\mu)+z(2v-\mu)]zdz = -B_{42}$$

$$B_{11} = B_{12} = B_{21} = B_{22} = B_{33} = B_{34} = B_{43} = B_{44} = 0$$

$$C_{22} = -R\mu\int_{-h/2}^{h/2}\left(\frac{R+z}{r_i}\right)^n\left(1+\frac{z}{R}\right)dz$$

$$C_{33} = -v \int_{-h/2}^{h/2} \left(\frac{R+z}{r_i}\right)/(R+z)dz$$

$$C_{34} = -v \int_{-\frac{h}{2}}^{\frac{h}{2}} \left(\frac{R+z}{r_i}\right)^n dz - (1-v) \int_{-\frac{h}{2}}^{\frac{h}{2}} \left(\frac{R+z}{r_i}\right)^n \left(\frac{z}{R+z}\right) dz = \ C_{43}$$

$$C_{44} = -2v \int_{-\frac{h}{2}}^{\frac{h}{2}} \left(\frac{R+z}{r_i}\right)^n zdz$$

$$- (1-v) \int_{-\frac{h}{2}}^{\frac{h}{2}} \left(\frac{R+z}{r_i}\right)^n \left(\frac{z^2}{R+z}\right) dz$$

$$- \ R(1-v) \int_{-\frac{h}{2}}^{\frac{h}{2}} \left(\frac{R+z}{r_i}\right)^n \left(1+\frac{z}{R}\right) dz$$

$$C_{11} = C_{12} = C_{13} = C_{14} = C_{21} = C_{23} = C_{24} = C_{31} = \ C_{32} = C_{41} = C_{42} = 0$$

$$\mu = \frac{K}{2}(1-2v)$$

Here *K* is the shear correction factor with a value of 5/6 for a cylinder.

APPENDIX B

The FGM cylinder under unsteady general heat transfer is modelled by FEM numerically. The robust commercial software, ABAQUS CAE is used to simulate the problem. Due to the axisymmetric nature of the problem a section of cylinder is modeled. In this simulation the ABAQUS 8-node coupled temperature and displacement (CAX8T) element is used. Radial variation of FGM mechanical and thermal properties is simulated in ABAQUS by defining the function in terms of radius in accordance with Eqns. (11)-(15). All thermal and mechanical boundary conditions defined earlier are implemented in the simulation. A snapshot of the simulation is shown in Fig. 17.

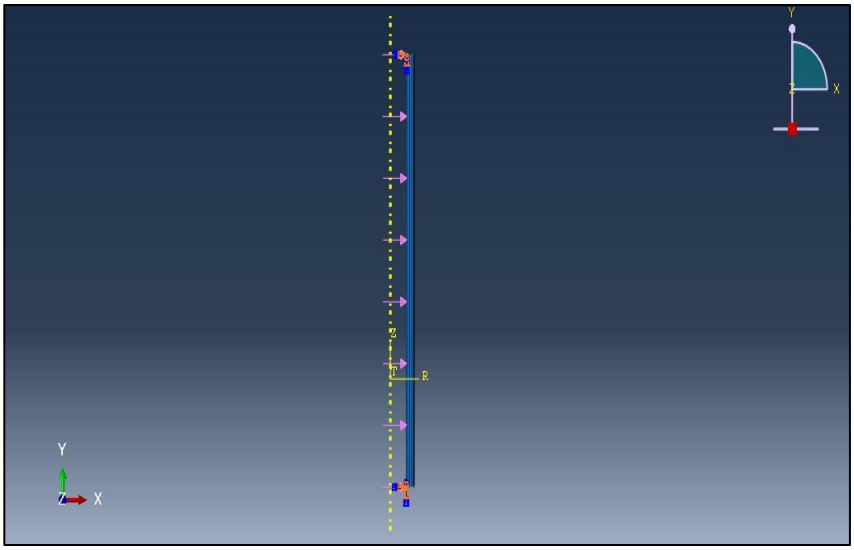

Fig. 17 ABAQUS simulation of FGM thick-walled cylinder

REFERENCES

[1] Xiang, H., Shi, Z. and Zhang, T., 2006. Elastic analyses of heterogeneous hollow cylinders. *Mechanics Research Communications*, 33(5), pp.681-691.

[2] Shi, Z., Zhang, T. and Xiang, H., 2007. Exact solutions of heterogeneous elastic hollow cylinders. *Composite structures*, 79(1), pp.140-147.

[3] Ghannad, M. and Nejad, M.Z., 2012. Complete elastic solution of pressurized thick cylindrical shells made of heterogeneous functionally graded materials. *Mechanics*, 18(6), pp.640-649.

[4] Xin, L., Dui, G., Yang, S. and Zhang, J., 2014. An elasticity solution for functionally graded thick-walled tube subjected to internal pressure. *International Journal of Mechanical Sciences*, 89, pp.344-349.

[5] Ghannad, M. and Nejad, M.Z., 2012. Elastic analysis of heterogeneous thick cylinders subjected to internal or external pressure using shear deformation theory. *Acta Polytechnica Hungarica*, 9(6), pp.117-136.

[6] Eipakchi, H.R., Rahimi, G.H. and Esmaeilzadeh, K., 2003. Closed form solution for displacements of thick cylinders with varying thickness subjected to non-uniform internal pressure. *Structural Engineering and Mechanics*, 16(6), pp.731-748.

[7] Ghannad, M., Rahimi, G.H. and Nejad, M.Z., 2013. Elastic analysis of pressurized thick cylindrical shells with variable thickness made of functionally graded materials. *Composites Part B: Engineering*, 45(1), pp.388-396.

[8] Belabed, Z., Houari, M.S.A., Tounsi, A., Mahmoud, S.R. and Bég, O. Anwar, 2014. An efficient and simple higher order shear and normal deformation theory for functionally graded material (FGM) plates. *Composites Part B: Engineering*, 60, pp.274-283.

[9] Zamani Nejad, M., Jabbari, M. and Ghannad, M., 2015. Elastic analysis of axially functionally graded rotating thick cylinder with variable thickness under non-uniform arbitrarily pressure loading. *International Journal of Engineering Science*, 89, pp.86-99.

[10] Arefi, M. and Rahimi, G.H., 2013. Thermo elastic analysis of a functionally graded cylinder under internal pressure using first order shear deformation theory. *Scientific Research and Essays*, 5(12), pp.1442-1454.

[11] Arani, A.G., Kolahchi, R. and Barzoki, A.M., 2011. Effect of material in-homogeneity on electro-thermo-mechanical behaviors of functionally graded piezoelectric rotating shaft. *Applied Mathematical Modelling*, 35(6), pp.2771-2789.

[12] Keles, I. and Conker, C., 2011. Transient hyperbolic heat conduction in thick-walled FGM cylinders and spheres with exponentially-varying properties. *European Journal of Mechanics-A/Solids*, 30(3), pp.449-455.

[13] Jabbari, M., Meshkini, M., Eslami, M.R., 2011. Mechanical and thermal stresses in a FGPM hollow cylinder due to radially symmetric loads. *ISRN Mechanical Engineering*, Article ID 291409, 1–9. doi:10.5402/2011/291409

[14] Kim, K.S. and Noda, N., 2002. A Green's function approach to the deflection of a FGM plate under transient thermal loading. *Archive of Applied Mechanics*, 72(2-3), pp.127-137.

[15] Jabbari, M., Sohrabpour, S. and Eslami, M.R., 2003. General solution for mechanical and thermal stresses in a functionally graded hollow cylinder due to non-axisymmetric steady-state loads. *ASME Journal of Applied Mechanics*, 70(1), pp.111-118.

[16] Shao, Z.S., 2005. Mechanical and thermal stresses of a functionally graded circular hollow cylinder with finite length. *International Journal of Pressure Vessels and Piping*, 82(3), pp.155-163.

[17] Jabbari, M., Bahtui, A. and Eslami, M.R., 2009. Axisymmetric mechanical and thermal stresses in thick short length FGM cylinders. *International Journal of Pressure Vessels and Piping*, 86(5), pp.296-306.

[18] Malekzadeh, P., Golbahar Haghighi, M.R. and Heydarpour, Y., 2012. Heat transfer analysis of functionally graded hollow cylinders subjected to an axisymmetric moving boundary heat flux. *Numerical Heat Transfer, Part A: Applications*, 61(8), pp.614-632.

[19] Ootao, Y., Tanigawa, Y. and Fukuda, T., 1991. Axisymmetric transient thermal stress analysis of a multilayered composite hollow cylinder. *Journal of Thermal Stresses*, 14(2), pp.201-213.

[20] Hosseini, S.M. and Akhlaghi, M., 2009. Analytical solution in transient thermo-elasticity of functionally graded thick hollow cylinders (Pseudo-dynamic analysis). *Mathematical Methods in the Applied Sciences*, 32(15), pp.2019-2034.

[21] Ghannad, M. and Yaghoobi, M.P., 2017. 2D thermo elastic behavior of a FG cylinder under thermomechanical loads using a first order temperature theory. *International Journal of Pressure Vessels and Piping*, 149, pp.75-92.

[22] Chaht, F.L., Kaci, A., Houari, M.S.A., Tounsi, A., and Bég, O. Anwar and Mahmoud, S.R., 2015. Bending and buckling analyses of functionally graded material (FGM) size-dependent nanoscale beams including the thickness stretching effect. *Steel and Composite Structures*, 18(2), pp.425-442.

[23] Mirsky I., and Hermann G., 1958. Axially motions of thick cylindrical shells, *ASME J. Appl. Mech*.; 25, pp. 97-102.

[24] Afshin, A., Zamani Nejad, M., and Dastani, K., 2017. Transient thermoelastic analysis of FGM rotating thick cylindrical pressure vessels under arbitrary boundary and initial conditions. *Journal of Computational Applied Mechanics*, 48(1), pp.15-26.

[25] Raminnia, M., Ghorbanpour, A. A., and Manouchehrifar, A., 2013. Thermo-mechanical nonlinear vibration in nano-composites polyethylene shell reinforced by CNT's embedded elastic. *International Journal of Advanced Design and Manufacturing Technology*, 6(4), pp. 91-97.

[26] Pourasghar, A., Moradi-Dastjerdi, R., Yas, M. H., Ghorbanpour Arani, A., and Kamarian, S., 2018. Three-dimensional analysis of carbon nanotube-reinforced cylindrical shells with temperature-dependent properties under thermal environment. *Polymer Composites*, 39(4), 1161-1171.

[27] Sepiani, H. A., Rastgoo, A., Ebrahimi, F., and Arani, A. G., 2010. Vibration and buckling analysis of two-layered functionally graded cylindrical shell, considering the effects of transverse shear and rotary inertia. *Materials & Design*, 31(3), 1063-1069.

[28] Sepiani, H., Rastgoo, A., Ahmadi, M., Ghorbanpour Arani, A., and Sepanloo, K., 2009. Elastic stability analysis of a two-layered functionally graded cylindrical shell under axial compression with the use of energy approach. *Advanced Composites Letters*, 18(6), 207-217.